Stress Corrosion Cracking Behavior of 4.19%Zn-1.34%Mg (A7N01S-T5) Aluminum Alloy Welded Joints

Guoqing Gou,[‡,*,**] Jia Chen,[*,***] Zhirui Wang,[**] Hui Chen,[*] Chuanping Ma,[*] and Peng Li[****]

ABSTRACT

The fracture toughness behavior of Al-Zn-Mg alloy, A7N01S-T5, welded joints was investigated using three points bending test with the J integral approach. The microstructures of the welded joints were examined using optical microscopy, microhardness, and transmission electron microscopy. The heat affected zone (HAZ) had the best crack propagation resistance, and the weld zone (WZ) and base metal (BM) behaved similarly. The stress corrosion cracking (SCC) behavior of the welded joints was investigated under a constant loading condition. The threshold stress intensity factor of SCC and the cracks' propagation rate were tested. The microstructure of the fracture was examined using optical microscope and scanning electron microscope. The results showed that both the BM and the HAZ were susceptible to SCC and the HAZ was smaller than the BM, but no cracks were detected in the WZ. A greater amount of H^+ and a higher concentration of Zn and Mg accumulated at the crack front tips, which led to the SCC resistance weakening in the A7N01S-T5 welded joints.

KEY WORDS: A7N01S-T5 aluminum alloy, cracking, fracture mechanics, stress corrosion cracking, threshold stress intensity, welded joints

INTRODUCTION

A7N01S-T5 aluminum alloy is an Al-Zn-Mg alloy that may be heat treated to have a yield strength as high as 300 MPa to 450 MPa with very good ductility. The alloy can be extruded into thin-walled and complex shapes. In addition, the alloy has excellent aging characteristics and weldability.[1] Specifically, the reduced strength from welding-induced softening can be restored through proper aging treatment. As a result, this alloy has been selected extensively for important structures in high-speed trains, including underframes, threshold, corbels, section beams, and end walls.[2]

The A7N01S-T5 alloy contains, in addition to Zn and Mg, various alloying elements such as Cu, Si, and Cr. It has been reported that when the Zn and Mg content was increased to the limit of Zn + Mg = 7.5% for solid solution strengthening, the sensitivity of the alloy to stress corrosion cracking (SCC) would increase considerably.[3-6] Increased temperature and humidity would also influence the SCC behavior of A7N01, especially when the concentration of chlorine ions in the atmosphere is relatively high and the pH value is low.[4]

Previous results also showed that the mechanism of SCC is related to the migration of corrosion products on metal surface.[7-9] When aluminum alloys and their welded joints are in corrosive atmosphere, low melting point compounds may form easily and may promote the occurrence of SCC. Others reported that the mechanism of SCC involves anodic dissolution.[10-13] Grain boundary precipitation usually plays the role of

Submitted for publication: January 28, 2016. Revised and accepted: May 11, 2016. Preprint available online: May 11, 2016, http://dx.doi.org/10.5006/2043.

‡ Corresponding author. E-mail: gouguoqing1001@163.com.
* School of Materials Science and Engineering, Southwest Jiaotong University, Sichuan, Chengdu 610031, China.
** Department of Materials Science and Engineering, University of Toronto, Ontario, Toronto M3S 5E4, Canada.
*** Chengdu Industry and Trade College, Sichuan, Chengdu 611731, China.
**** CSR Qingdao Sifang Co. Ltd, Shandong, Qingdao 266000, China.

ISSN 0010-9312 (print), 1938-159X (online)

TABLE 1
Chemical Concentration of A7N01S-T5 Alloy and AA5356 Welding Wire

Materials	Chemical Content (wt%)									
	Zn	Mg	Cu	Mn	Cr	Ti	Zr	Si	Fe	Al
A7N01[A]	4.190	1.340	0.011	0.317	0.233	0.043	0.122	0.046	0.100	Bal.
JISH 4000-2006[B]	4.0 to 5.0	1.0 to 2.0	<0.2	0.2 to 0.7	<0.30	<0.20	<0.25	<0.3	<0.35	Bal.
AA5356[C]	≤0.10	4.5 to 5.5	≤0.10	0.05 to 0.20	0.05 to 0.20	0.06 to 0.2	–	≤0.25	≤0.10	Bal.

[A] A7N01: the aluminum alloy base metal used in the present investigation.
[B] JISH 4000-2006: the corresponding Japanese Al alloy with the Japanese Industrial Standard (JISH 4000-2006).
[C] AA5356: the welding wire material used in the present research.

TABLE 2
Mechanical Properties of A7N01S-T5 and JISH 4100-2006

Materials	Hardness (HV)	Tensile Strength (MPa)	Yield Strength (MPa)	Elongation (%)	Impact Toughness (J/cm^2)	Fatigue Limit (MPa)
A7N01S-T5	107	393	327	15.5	24	174.5
JISH 4100-2006[A]	–	≥325	≥245	≥10	–	–

[A] JISH 4000-2006: the corresponding Japanese Al alloy with the Japanese Industrial Standard (JISH 4000-2006).

TABLE 3
Welding Processing Parameters for A7N01S-T5 Alloy[A]

Materials	Thickness (mm)	Weld	Peak Current (A)	Voltage (V)	Welding Speed (mm/min)	Gas Flow (L/min)	Environment Temperature (°C)	Environment Humidity (%)
A7N01S-T5	10	1	205	20	350	25	24 to 26	50
	10	2	210	20	330	25	24 to 26	50

[A] The gas used for welding was 999.99% purity argon.

anode and would be dissolved first when the service condition is corrosive. However, other reports firmly demonstrated that the SCC phenomenon is a result of the hydrogen-induced SCC.[14-28] As SCC proceeds, the reduced H atoms would form H_2 bubbles generating crack along the grain boundaries.

SCC is considered to be a very dangerous form of failure to the safety of high-speed train structures. A number of A7N01 Al alloy components such as traction beams, bumper beams, and cross beams, as well as many other aluminum alloy structures manufactured with A7N01 aluminum alloys, experience fracture from time to time. Many of these failures result from SCC. The present research group has demonstrated in previous publications that the features of those cracks were consistent with SCC.[29-34]

This paper reports the results from an investigation on the critical threshold stress intensity factor for SCC (K_{ISCC}) and crack propagation data.

MATERIALS AND METHODS

Materials and Welding Parameters

The testing materials used were A7N01S alloy plates of 10 mm thickness under T5 aging condition (cooled down from an elevated temperature forming process and then artificially aged according to ISO Standard 2107:2007[35]). Welding was performed by the metal inert gas technique with a PHOENIX 421 EXPERT[†] welding machine. The welding wires were ER5356 (AA5356, UNS A95356[(1)]) of 1.6 mm diameter. The chemical compositions of the A7N01S Al alloy base metal, A7N01S, and the welding wire are listed in Table 1. The mechanical properties of A7N01S under the T5 condition are listed in Table 2. The welding parameters are listed in Table 3. To remove the oxides and reduce the porosity of the joint, the surface of the alloy was chemically cleaned before welding.

Fracture Toughness Test

Samples were fabricated from the base metal (designated as BM), heat affected zone (HAZ), and welded zone (WZ) of the welded joints according to the standards of ISO Standard 12135:2002.[36] The sample direction was perpendicular to the welded seam, as

[†] Trade name.
[(1)] UNS numbers are listed in *Metals and Alloys in the Unified Numbering System*, published by the Society of Automotive Engineers (SAE International) and cosponsored by ASTM International.

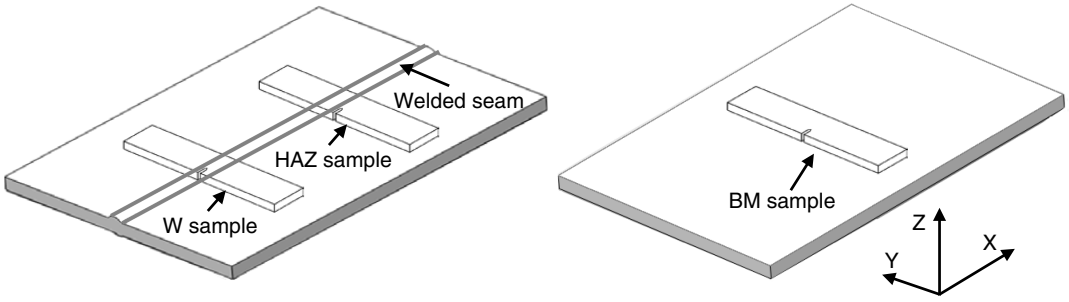

FIGURE 1. *Sample cutting layout for fracture toughness test.*

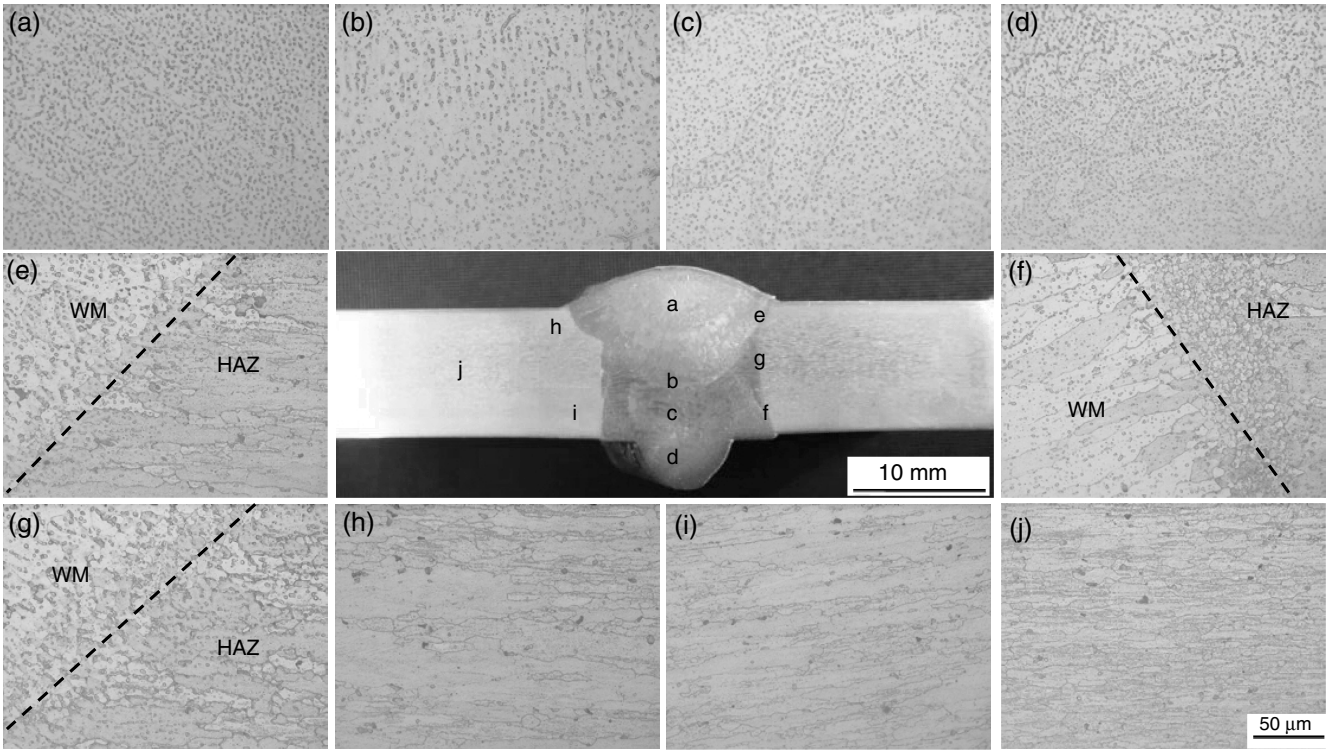

FIGURE 2. *Optical micrograph of welded joints.*

shown in Figure 1. The HAZ and WZ region samples were cut based on the optical microstructure observation, as well as the microhardness distribution.

The microstructures of WZ, HAZ, and BM regions are shown in Figure 2. The elongated grains from rolling were clearly seen in both HAZ and BM regions. The microstructure consisted of recrystallized grains with undissolved phases and impurity particles. The microstructure of BM was similar to that of the HAZ. In the WZ region, there were uniformly distributed equiaxed grains whose sizes were smaller than in the HAZ and BM regions. Figure 3 shows that the hardness in the WZ region was lower than in the BM and HAZ.

Figure 4 presents the transmission electron microscope (TEM) micrographs taken in the welded joints by a JEM-2010† microscope. Precipitated particles can be seen everywhere, including within grains

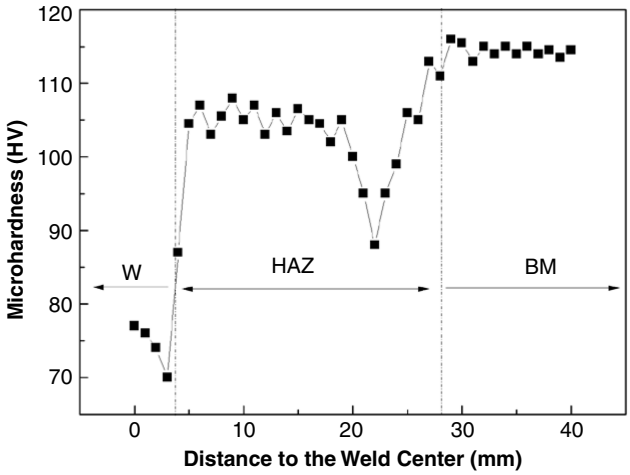

FIGURE 3. *Microhardness distribution from weld zone to base metal.*

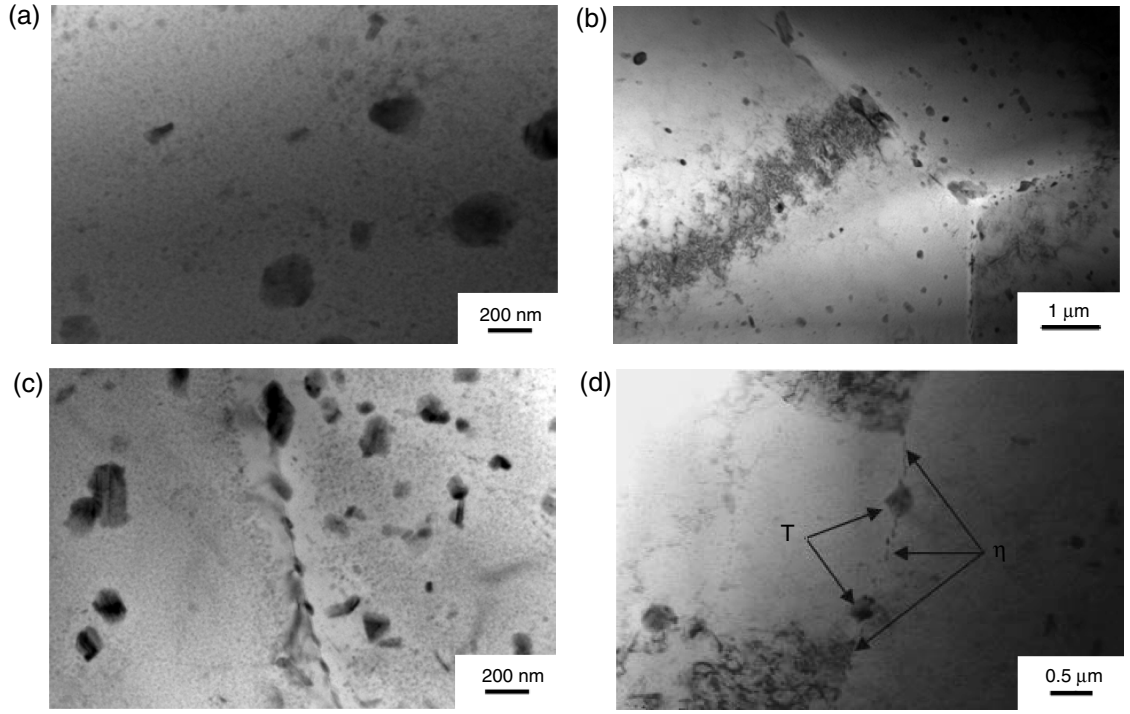

FIGURE 4. *TEM microstructures of welded joints.*

(Figure 4[a]) and along grain boundaries (Figures 4[c] and [d]). The large particles seen in Figures 4(c) and (d) along the grain boundaries are believed to be either T($A1_2Mg_2Zn_3$) or η($MgZn_2$) phase particles.[37] Many small precipitates are also seen distributed along the grain boundaries, which appear to be associated with the large particles. The size of precipitate-free zone (PFZ) was estimated to be 80 mm to 90 nm. As reported previously, the wider the PFZ region, the greater the stress corrosion resistance of the materials.[38]

Figure 5 presents the sample design for three points bending test, and the test was conducted with a WD-E† electronic universal test machine. A sharp incision was machined at the edge of the samples using electron discharge machining. The diameter of the molybdenum cutting wire was 0.14 mm. Precracks were introduced by a cyclic deformation process with a YK-I† dual elastic fork fatigue machine. The precrack length was generally 3 mm to 5 mm long, and the effective length of the cracks was controlled to satisfy $0.45 \leqq a/W \leqq 0.70$.

The fracture toughness in the present investigation was obtained using J integral approach. The test was done in air; the atmosphere was 50% humidity and the temperature was 24°C to 26°C. The equation for J integral approach calculation is:

$$J_0 = J_e + J_p = \left[\frac{FS}{(BB_N)^{0.5} W^{1.5}} \times g_1\left(\frac{a_0}{W}\right)\right]^2 \left[\frac{1-\upsilon^2}{2R_{p0.2}E}\right] + \frac{2U_p}{B_N(W-a_0)} \quad (1)$$

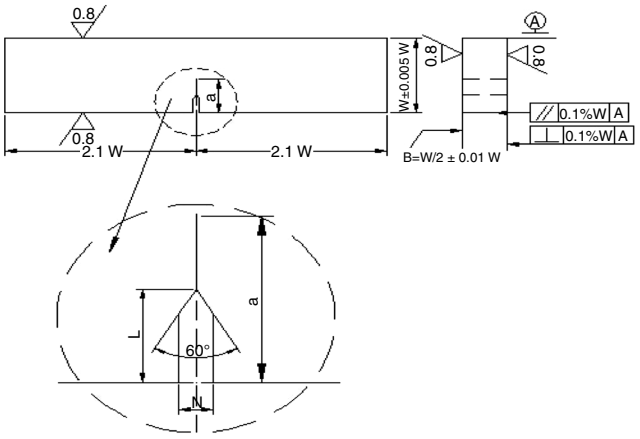

FIGURE 5. *Sample design for three point bending fracture toughness test (unit: mm).*

where J_0 is the experiment component of J integral in kJ/m^2, J_e is the elastic component of J integral in kJ/m^2, J_p is the plastic component of J integral in kJ/m^2, F is the applied load in kN, S is the loading span in mm, B is the thickness of the sample in mm, B_N is the net thickness of the sample between the slots on both sides in mm, W is the width of the sample in mm, g_1 is the constant in the standard according to the sample size, a_0 is the initial crack length in mm, υ is Poisson's ratio = 0.3, $R_{p0.2}$ is the nonproportional extension strength that is perpendicular to the crack plane under the experiment temperature (equal to 327.7 MPa), E is the modulus of elasticity in GPa, and

U_p is the energy of plastic deformation component that was obtained by considering the region enclosed by the loading and displacement curve in J. This equation and testing method is in accordance with the ISO Standard 12135:2002.[36]

Stress Corrosion Cracking Test

Samples in the direction of Y-Z (see Figure 1) for SCC testing were cut and machined from the BM, HAZ, and WZ of the welded joints according to ISO Standard 7539-6:2003[39] and ISO Standard 7539-8:2000.[40] A notch was cut at the edge of each sample the same way as the fracture toughness test samples. The presetting notch was 2 mm long and the precrack length was 6 mm long.

To assure the accuracy of the testing data, only the region of interest of each sample was immersed into the solution during testing, and the rest of the sample surface was masked with the BONLE type cyanoacrylate adhesive glue. The sharp incision and the extensometers were also isolated using glue and then covered with epoxy. A paper cup was used as the corrosion solution container. The entire setup for the SCC testing is shown in Figure 6.

The SCC tests were conducted at a constant load using a cantilever beam on a CFW-150† SCC testing machine. Samples were immersed in 3.5%NaCl solution at a temperature of 45±1°C (Figure 6). One drop of the solution was added into the solution container by an infusion catheter every 30 s. Such a rate of solution addition was approximately equal to the evaporation rate of the solution, so the solution remained at the same level in the container.

At first, a preset test time period of 72 h was selected for the SCC testing. The crack opening displacement, δ, was monitored during the test with an extensometer and, therefore, the crack propagation time could be obtained by the δ-t curve. However, if the δ-t curve did not demonstrate any apparent change in the first 72 h, the testing time was extended to 144 h or even longer, with the longest time used being 228 h when the test ended. The surface crack length was measured with an optical measuring microscope. If the sample had not failed, it was pulled apart using a tension machine. This test was according to ISO Standard 7539-6:2003.[39]

The initiation crack length a_0 was measured in five places along the thickness direction of the sample fracture, which were the left edge of the fracture, 0.25 times the thickness of the sample from the left edge of the fracture, 0.5 times the thickness of the sample from the left edge of the fracture, 0.75 times the thickness of the sample from the left edge of the fracture, and the right edge of the fracture. If the results were obtained before the SCC test, the average value of the above five values was considered as the initiation crack length, a_0. If the results were obtained after the SCC test, the average value of the above five values was considered as the final crack length, a_f. The measuring sketch map is shown in Figure 7.

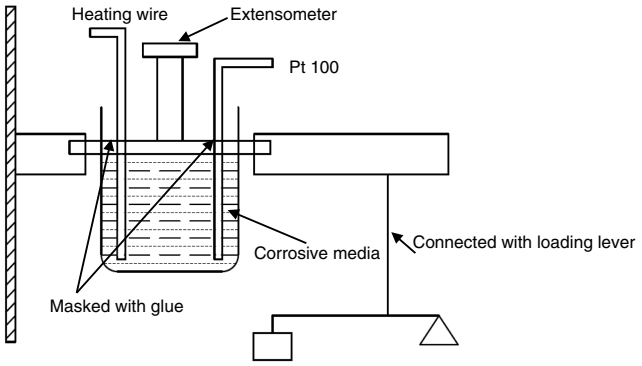

FIGURE 6. *SCC testing setup and the corresponding schematic diagram.*

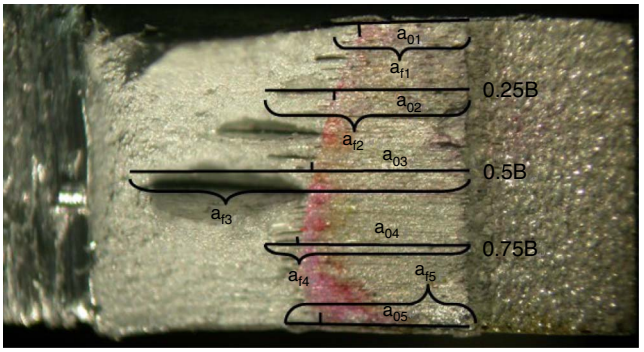

FIGURE 7. *Sketch map of the crack length measurement.*

The bending moment of the test was obtained from K_{Ii} (Equation [2]):

$$M = \frac{K_{Ii} B W^{\frac{3}{2}}}{4.12(\alpha^{-3} - \alpha^{3})^{\frac{1}{2}}} \quad (2)$$

where M is the bending moment in N·m; K_{Ii} is the stress intensity factor, obtained from the beginning of stress corrosion cracking in MPa$\sqrt{m}$; and $\alpha = 1 - \frac{a}{W}$. The other variables in Equation (2) are listed in Equation (1).

The sample sizes met the plane strain condition as governed by Equation (3):

$$B \geq 2.5(K_{ISCC}/\sigma_{0.2})^2 \quad (3)$$

where K_{ISCC} is the threshold stress intensity factor for stress corrosion cracking in MPa$\sqrt{m}$ and $\sigma_{0.2}$ is the yield strength in MPa. The other variables in Equation (2) are listed in Equation (1).

The force from the loading lever P is obtained from (4):

$$P = \frac{M - M_0}{S} \quad (4)$$

where P is the force from the loading lever in MPa; M_0 is the constant bending moment resulting from the testing machine weight, $M_0 = 6.9$ N·m; and S is the distance of the center crack to the load point line of the loading lever in mm. Note: Equations (2) through (4) are all from ISO Standard 7539-6:2003.[39]

Microstructures After Stress Corrosion Cracking Test

The microscopic structures of the samples were observed by a stereo microscope, as well as a JSM-6490LV† scanning electron microscope (SEM) with Genesis 2000† energy dispersive x-ray spectrometer (EDS) to analyze the chemistry of the samples.

RESULTS AND DISCUSSION

Fracture Toughness

The results of the J integral measurements are shown in Table 4 and Figure 8.

There were seven samples tested for each of the three zones, i.e., BM, HAZ, and WZ. The J integral of the HAZ samples seem to be the highest, and the WZ samples the lowest, with the BM samples in between. A lognormal distribution method was used to evaluate the results using the equation:[41]

$$f(x) = \frac{1}{x\zeta\sqrt{2\pi}} \exp\left[-\frac{(\ln x - \lambda)^2}{2\zeta^2}\right] \quad (5)$$

where λ is the average value of ln x and ζ is the standard deviation of ln x.

The J_0 values of HAZ, WZ, and BM were found to be 71.7 kJ/m^2, 53.63 kJ/m^2, and 51.7 kJ/m^2, respectively. Thus, the HAZ had the best crack propagation resistance, and the WZ and the BM were similar and lower.

K_{ISCC} and da/dt

During testing, the applied load used in different samples was in accordance with ISO Standard 7539-1:2012.[42] It was found that the longest time was 228 h, at which time the recorded K_{Ii} value was taken as K_{ISCC}. For different testing conditions, the value of K_{Ii} was calculated with the use of Equation (6):

$$K_{Ii} = \frac{4.12(PS + M_0)(\alpha^{-3} - \alpha^3)^{\frac{1}{2}}}{BW^{\frac{3}{2}}} \quad (6)$$

Note: Equation (6) is from ISO Standard 7539-1:2012[42] and all variables have been described in Equations (1) through (4).

The summary of the SCC test results for the A7N01S-T5 joints are presented in Table 5 and Figure 9. The fitting equations (Equations [7] and [8]) are obtained through the analysis of first-order nonlinear exponential decay regression.

$$y_{BM} = 46.50 \times \exp\left(-\frac{x}{27.84}\right) + 15.41 \quad (7)$$

$$y_{HAZ} = 45.94 \times \exp\left(-\frac{x}{17.57}\right) + 14.03 \quad (8)$$

It is interesting to see that cracks were detected to have initiated in both BM and HAZ samples, but there

TABLE 4
J Integral Results

No.	W (mm)	B (mm)	a/Initial (mm)	F (kN)	a_0/W	g_1 (a_0/W)	U_p (kJ)	Je (kJ/m^2)	J_p (kJ/m^2)	J_0 (kJ/m^2)
BM-1	24.07	12.42	14.02	5.66	0.58	3.53	2.07	21.91	33.24	55.15
BM-2	24.07	12.38	14.97	4.69	0.62	4.11	1.83	20.56	32.44	53.00
BM-3	24.01	12.39	15.68	4.00	0.65	4.69	1.75	19.56	33.91	53.47
BM-4	24.01	12.94	12.74	7.15	0.53	2.94	1.99	22.48	27.25	49.73
BM-5	24.01	12.45	14.79	5.08	0.62	4.01	1.74	22.94	30.24	53.18
BM-6	24.01	12.26	13.69	6.25	0.57	3.38	1.57	24.50	24.86	49.36
BM-7	23.81	12.31	12.46	7.12	0.52	2.87	2.04	23.42	29.20	52.62
HAZ-1	23.97	12.40	13.48	4.74	0.56	3.28	4.58	13.47	70.36	83.82
HAZ-2	24.05	12.43	13.63	4.80	0.57	3.35	4.22	14.15	65.24	79.39
HAZ-3	24.05	12.45	16.67	2.63	0.69	5.65	2.46	11.70	53.56	65.26
HAZ-4	23.84	12.41	4.39	14.41	0.60	3.84	2.73	16.10	46.64	62.73
HAZ-5	23.83	12.31	13.54	4.70	0.57	3.35	4.01	14.32	63.26	77.58
HAZ-6	23.91	12.43	12.91	5.63	0.54	3.04	3.44	16.34	50.38	66.72
HAZ-7	23.95	12.48	12.59	6.11	0.53	2.89	4.34	16.73	61.22	77.95
W-1	24.03	12.53	14.41	3.20	0.60	3.77	2.73	7.86	45.30	53.16
W-2	24.05	12.71	13.65	3.79	0.57	3.35	2.52	8.44	38.23	46.67
W-3	24.05	12.48	13.84	3.61	0.58	3.44	2.41	8.43	37.75	46.18
W-4	24.01	12.39	14.22	3.39	0.59	3.66	2.96	8.57	48.90	57.47
W-5	23.91	12.50	14.40	3.25	0.60	3.81	2.74	8.49	46.15	54.64
W-6	24.02	12.39	13.29	4.43	0.55	3.18	2.54	10.67	38.16	48.83
W-7	23.89	12.10	13.66	3.70	0.57	3.40	2.48	9.08	40.08	49.16

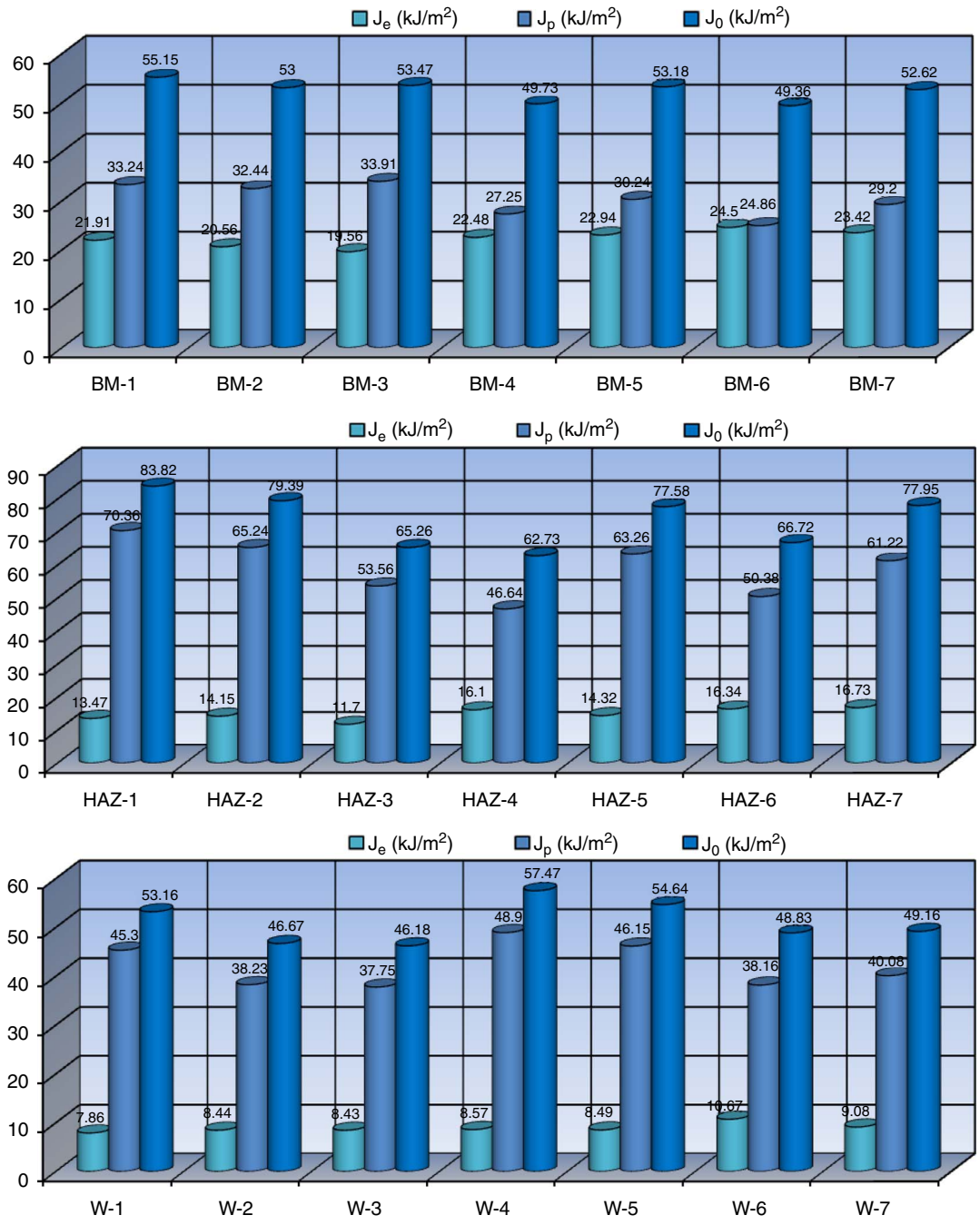

FIGURE 8. *J integral measurement results of welded joints.*

was no crack initiation detected in the WZ under the current testing condition. As the welding wire used was AA5356, the chemistry of the WZ was found to be similar to that of AA5083 (UNS A95083) Al alloy. Based on the results, it can be concluded that the WZ had the lowest SCC sensitivity among the three major regions, i.e., WZ, BM, and HAZ.

The crack initiation time vs. K_{Ii} curves are shown in Figure 9. Figure 10 shows a schematic figure for σ_{SCC} calculation. The stress at the crack tip can be calculated[43] with Equations (9) and (10), as well as Equation (2), assuming through thickness and that the crack is straight:

$$\sigma_{SCC} = \frac{M}{W_Z} \tag{9}$$

$$W_Z = \frac{B(W-a)^2}{6} \tag{10}$$

where σ_{SCC} is the critical threshold stress in MPa and W_Z is coefficient of bending section in mm^3. The other variables are listed in Equations (1) through (4).

TABLE 5
SCC Test Results

No.	W (mm)	B (mm)	a/Initial (mm)	a/After Corrosion (mm)	M (N·m)	K_{Ii} (MPa$\sqrt{m}$)	Crack Initiation Time (h)	Test Time (h)	a/W
BM-1	19.96	9.98	11.00	12.04	74.42	33.75	25.7	228	0.55
BM-2	19.88	9.98	10.88	11.26	63.54	28.81	35.2	87	0.55
BM-3	19.94	9.96	9.76	9.90	55.04	24.96	47.2	73	0.49
BM-4	19.82	10.00	10.02	10.11	45.44	20.60	53.3	72	0.51
BM-5	19.92	10.00	10.28	10.38	42.38	19.22	73.1	100	0.52
BM-6	19.88	10.00	10.82	11.13	36.85	16.71	108	208	0.54
BM-7	19.98	10.02	10.02	10.02	33.45	15.17	—	228	0.50
HAZ-1	19.98	10.04	11.00	12.27	80.88	36.68	12.8	107	0.55
HAZ-2	19.88	10.02	9.84	11.04	61.67	27.97	20	143	0.49
HAZ-3	19.92	10.02	10.00	10.33	41.53	18.83	37.6	74	0.50
HAZ-4	19.96	10.02	10.66	10.98	38.13	17.29	50.9	87	0.53
HAZ-5	19.98	10.00	10.96	11.43	37.7	17.10	55.4	189	0.55
HAZ-6	19.96	10.02	9.68	9.68	28.86	13.09	—	228	0.48
W-1	20.04	10.12	10.80	10.80	80.20	—	—	408	—
W-2	19.96	10.06	10.98	10.98	68.73	—	—	288	—
W-3	19.68	10.02	10.88	10.88	49.43	—	—	240	—

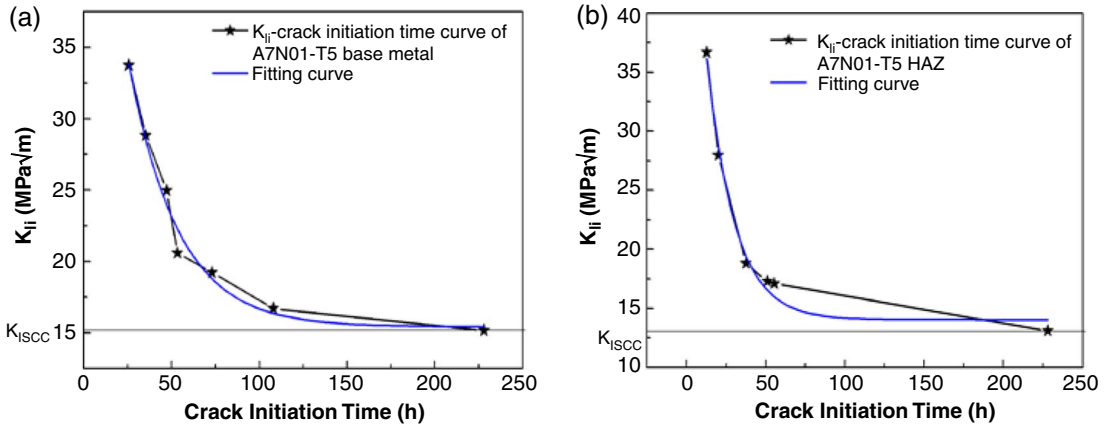

FIGURE 9. *The K_{Ii} and cracks initiation time relationship.*

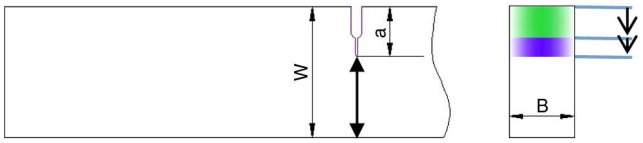

FIGURE 10. *Schematic for σ_{SCC} calculation, where the green region represents the sharp incision and the blue region represents the fatigue crack propagation zone.*

The threshold stress intensity factors K_{ISCC} of BM and HAZ were calculated to be 15.17 MPa$\sqrt{m}$ and 13.09 MPa$\sqrt{m}$, respectively. Compared with the fracture toughness results, the crack propagation resistance of HAZ was considerably lower than the BM during SCC testing. The σ_{SCC} of BM and HAZ was found to be 202 MPa and 164 MPa, respectively. Interestingly, in a previous investigation,[20] the σ_{SCC} values of BM and HAZ were found to be 0.62 times and 0.5 times the tensile strength of welded joints

TABLE 6
Crack Propagation Rate Results

No.	$(da/dt)_{av}$ with the Time of the Actual Expansion (mm/h)	$(da/dt)_{av}$ Throughout the Expansion (mm/h)
BM-1	5.14×10^{-3}	4.56×10^{-3}
BM-2	7.34×10^{-3}	4.37×10^{-3}
BM-3	5.22×10^{-3}	1.85×10^{-3}
BM-4	4.74×10^{-3}	1.23×10^{-3}
BM-5	3.75×10^{-3}	1.01×10^{-3}
BM-6	3.14×10^{-3}	2.91×10^{-3}
BM-7	—	4.38×10^{-6}
HAZ-1	13.5×10^{-3}	11.9×10^{-3}
HAZ-2	9.75×10^{-3}	8.38×10^{-3}
HAZ-3	9.05×10^{-3}	4.45×10^{-3}
HAZ-4	8.56×10^{-3}	3.63×10^{-3}
HAZ-5	3.50×10^{-3}	2.48×10^{-3}
HAZ-6	—	3.95×10^{-6}

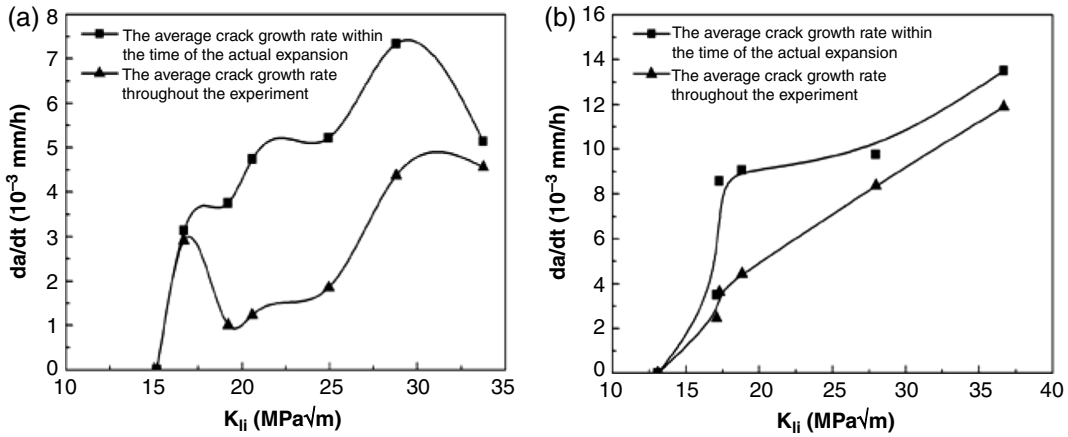

FIGURE 11. *Crack propagation rate, da/dt, of SCC for (a) BM and (b) HAZ.*

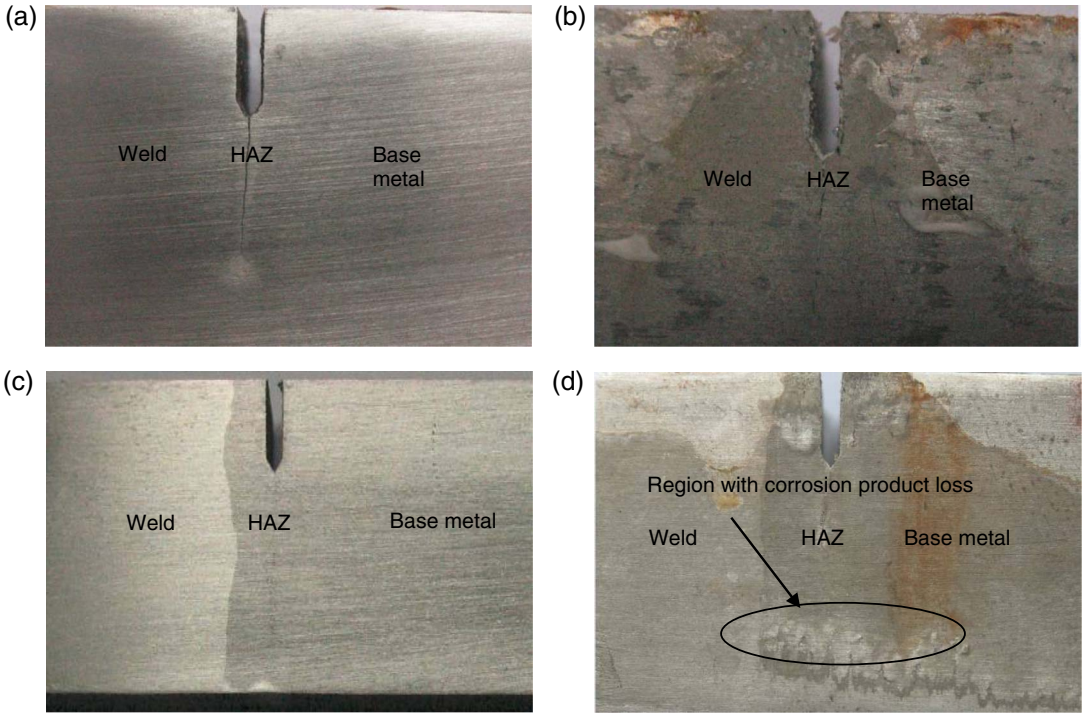

FIGURE 12. *Macroscopic morphology of samples.*

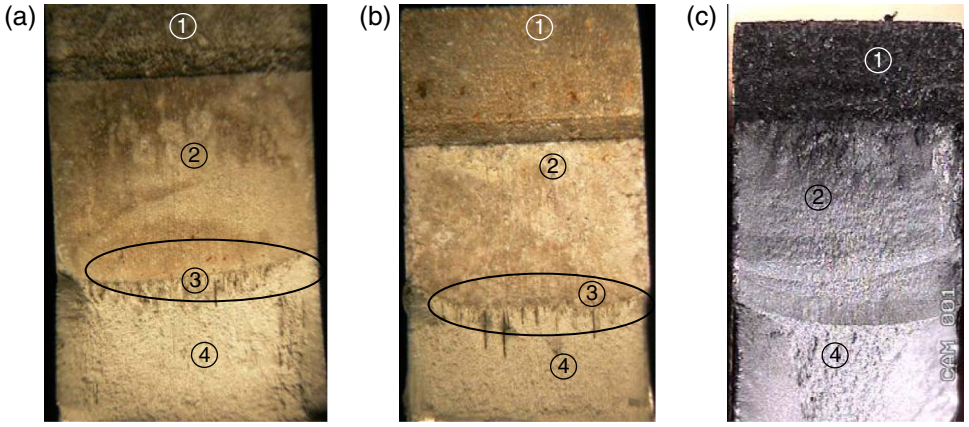

FIGURE 13. *Macroscopic morphology of fracture surface.*

(325 MPa), respectively. Furthermore, the ratio of HAZ σ_{SCC}/BM σ_{SCC} was 0.812, but the ratio of the HAZ K_{ISCC}/BM K_{ISCC} was 0.863. Both values were far from the value of $K_{IC.}$ The BM and the HAZ are both sensitive to SCC, but HAZ is apparently more sensitive to SCC than BM.

The crack propagation rate, da/dt, during SCC condition is shown in Table 6 and Figure 11.

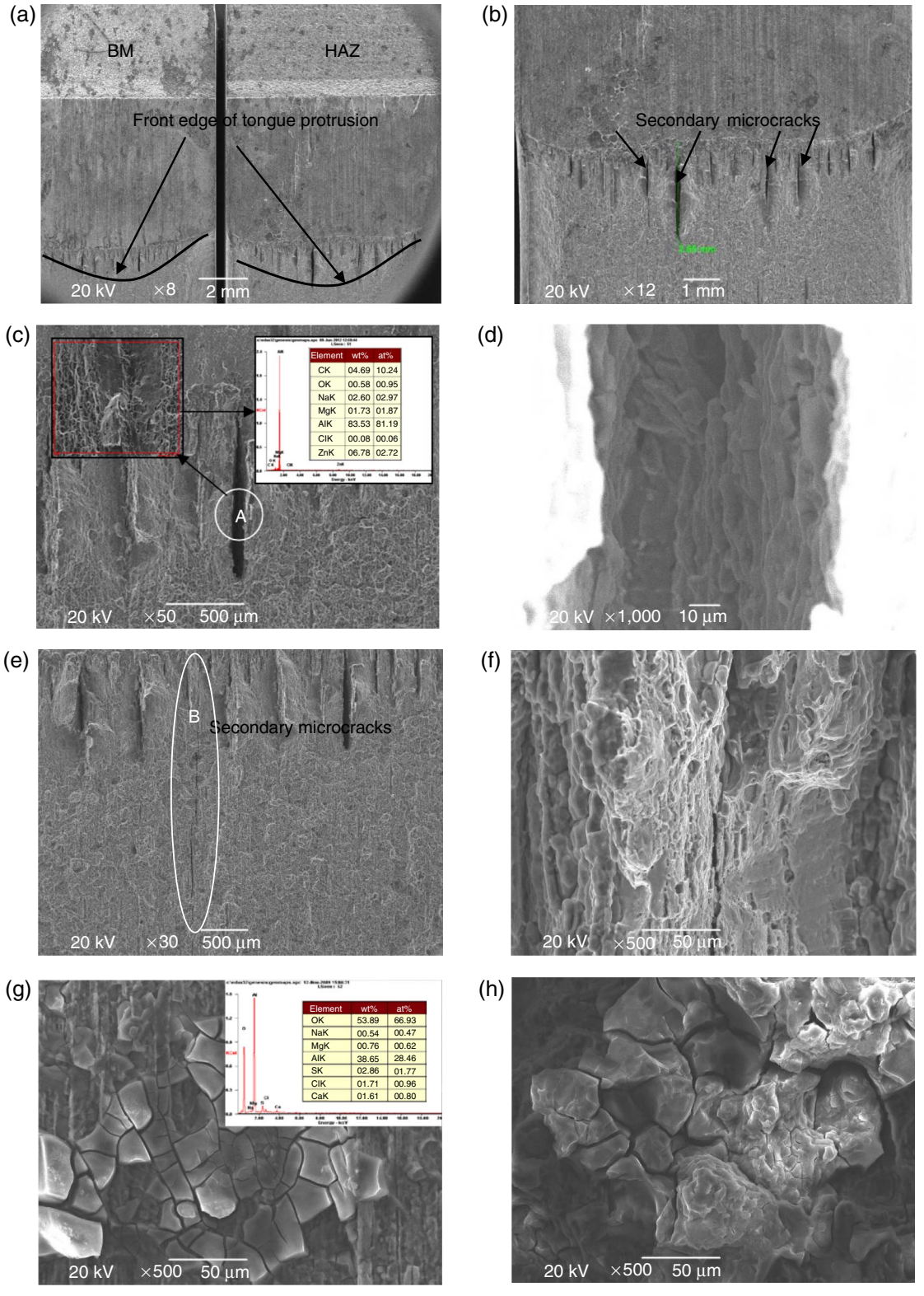

FIGURE 14. *Microstructures of fracture surface.*

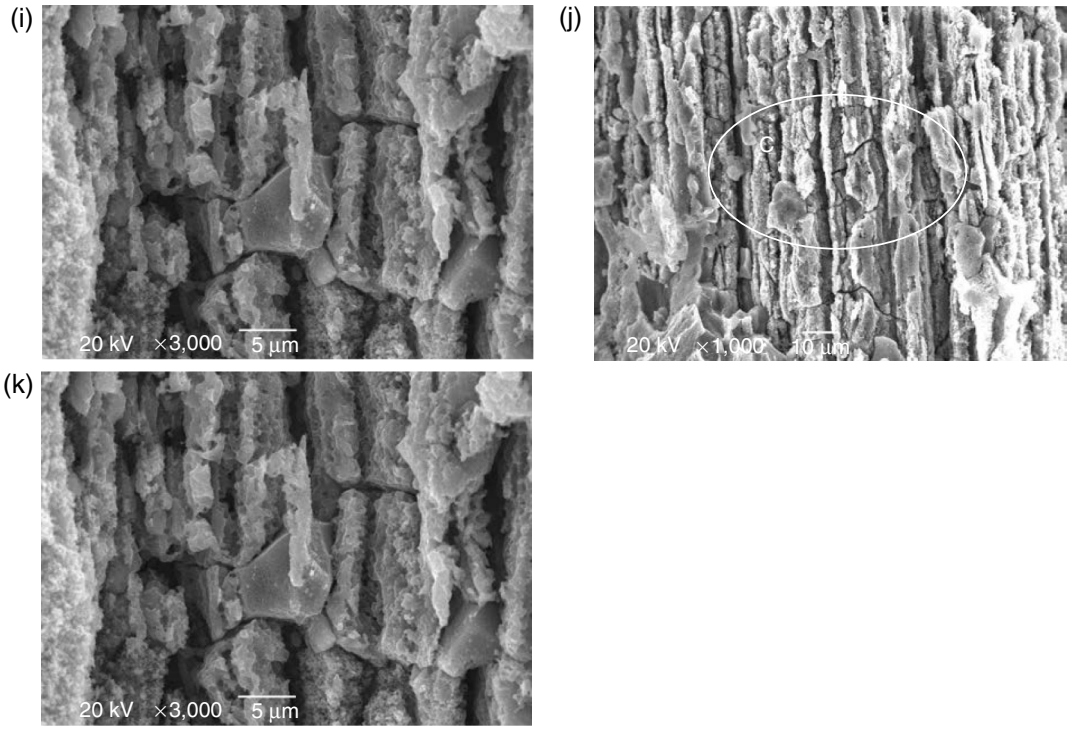

FIGURE 14. *(Continued).*

The crack propagation rate increased with increasing K_{Ii}, and the crack propagation rate in the HAZ was slightly higher than in the BM, with the da/dt value in HAZ equal to 3.95×10^{-6} mm/h compared to 4.4×10^{-6} mm/h in BM. The highest crack propagation rate was found to be 13.5×10^{-3} mm/h in the sample HAZ-1, with a corresponding K_{Ii} of 36.7 $MPa\sqrt{m}$. Hardwick, et al.,[25] showed that the residual stress in the HAZ was tensile, but was compressive in BM. The superposition of the applied stress and the residual stress in the HAZ region led to the highest sensitivity of this region to SCC crack propagation.

Microstructures After Stress Corrosion Cracking Test

Figure 12 shows the macroscopic morphology of cracks in BM and HAZ. There are obviously some corrosion products on the discolored sample surface and inside the notch. More severe discoloration can be seen as the yellow stain in the HAZ region (Figure 12[d]).

There are four different regions on the fracture surface in Figures 13(a) and (b), but only three regions in Figure 13(c). Specifically, the features of region 3 showed coarse morphology that was different from the other three regions: the line grooves with different lengths and tongue protrusions are not seen in other regions.

The SEM micrographs in Figure 14 show the fracture surface morphology. There was not much difference in fracture surface micromorphology. The fracture surfaces were rather flat, and the crack paths were all perpendicular to the loading direction.

Generally speaking, with samples used in the present investigation, the crack front tip in the sample thickness direction was closer to a plane strain state. The strain state concentration led to plastic deformation and prevented formation of the second passivation film at the crack front tip, so the crack front tip was still in the active state. The area in the crack front tip was larger than in the other location. For this reason, more H^+ assembled at the crack front tip. The concentration H^+ decreased the binding force of the atoms, and the binding energy was also decreased.[6,44-46] The microstructures at the end of the fatigue crack region and the entire front SCC showed a morphology of tongue protrusion, as seen in Figure 14(a). As the center of the crack front line was more a plane strain condition, the normal stress in the sample thickness direction became higher, leading to longer secondary cracks. In fact, the longest secondary crack in Figure 14(b) was measured to be 2.65 mm at the center of the crack front.

EDS analysis of the crack tips in region A of Figure 13(c) indicated that the main elements in this region were Al, Zn, Mg, Na, and Cl. Specifically, the weight percentage of Zn was approximately 7% and Mg was approximately 2%. The total amount of Zn and Mg was larger than the recommended standard composition in this Al alloy (see Table 1). This result indicates that a higher concentration of Zn and Mg exists in the crack front tip areas. Gou[47] showed that the SCC resistance became weaker when the total

concentration of Zn and Mg was higher than 7% for Al alloys.

CONCLUSIONS

The fracture toughness and the stress corrosion cracking behavior of A7N01S-T5 Al alloy welded joints were investigated. The threshold stress intensity factor K_{ISCC} for the SCC behavior and the crack propagation rate, da/dt, were examined. The microstructure and fracture surface morphology after SCC tested samples were also examined by various techniques. The conclusions were:

- The J_0 value of HAZ, WZ, and BM were found to be 71.67 kJ/m^2, 53.63 kJ/m^2, and 51.74 kJ/m^2, respectively. The HAZ had the highest crack propagation resistance, and the WZ was moderately better than the BM.
- The K_{ISCC} of BM and HAZ was found to be 15.17 MPa$\sqrt{m}$ and 13.09 MPa$\sqrt{m}$, respectively. The crack propagation rate of HAZ and BM was 3.95×10^{-6} mm/h and 4.38×10^{-6} mm/h, respectively. The BM and HAZ are more susceptible to SCC, with the HAZ having a higher susceptibility than BM. No apparent cracks were detected in WZ region in the SCC tests.
- The crack front tip is closer to a plane strain state, which led to plastic deformation and prevented the formation of the second passivation film, so the crack front tip was still in the active state with the larger area, which led to more H^+ assembling at the crack front tip.
- A higher concentration of Zn and Mg existing in the crack front tip areas would lead to the SCC resistance becoming weaker.

ACKNOWLEDGMENTS

The results of this paper were from multiple projects which include (i) “Effect of residual stresses on the corrosion behavior in weld joints and development of control technology for car bodies in aluminum-alloy trains,” (ii) “Research of the key technologies and equipment for next-generation railway transportation in cities,” and (iii) “Basic research of the design and advanced welding technology for high-speed trains in the wide region of environment.” The authors acknowledge the financial support from the Scientific and Technology Innovation Program of Chinese Central Universities (No. 2682014CX003), the National Science & Technology Pillar Program (No. 2015BAG12B01), and the National Key Basic Research and Development plan (No. 2014CB660807).

REFERENCES

1. X. Li, *Metallography and Microstructure of Aluminum Alloy Materials*, 4th ed. (Beijing, China: Metallurgical Industry, 2010).
2. Y. Wang, H. Chen, *Welding Technology of Aluminum Alloy Train Body for High Speed Trains*, 1st ed. (Chengdu, China: Southwest Jiaotong University, 2012).
3. L.X. Qian, *China Railway Sci.* 24 (2003): p. 1-11.
4. X.M. Wang, J.J. Zhao, G.Q. Gou, *Adv. Mater. Res.-Switz.* 239-242 (2011): p. 2822-2826.
5. H.P. Godard, W.B. Jepson, M.R. Bothwell, *Corrosion of Light Metals*, 1st ed. (New York, NY: John Wiley & Sons Inc., 1967).
6. L. Jihua, L. Di, G. Baolan, *Corros. Sci. Protect. Technol.* 16 (2001): p. 38-42.
7. R.J. Asaro, W.A. Tiller, *Metall. Trans.* 3 (1972): p. 1789-1796.
8. R. Nishimura, T. Yoshida, *Corros. Sci.* 50 (2008): p. 1205-1213.
9. K. Sieradzki, F.J. Friedersdorf, *Corros. Sci.* 36 (1994): p. 669-675.
10. H.A. Holl, *Corrosion* 23 (1967): p. 173-180.
11. A.J. DeArdo, R.D. Townsend, *Metall. Trans.* 1 (1970): p. 2573.
12. M. Landkof, L. Galor, *Corrosion* 36 (1980): p. 241-246.
13. Y. Uematsu, T. Kakiuchi, M. Nakajima, *Mater. Sci. Eng. A* 531 (2012): p. 171-177.
14. Y. Deng, B. Peng, G.F. Xu, Q.L. Pan, R. Ye, Y.J. Wang, L.Y. Lu, Z.M. Yin, *Corros. Sci.* 100 (2015): p. 57-72.
15. R. Nishimura, *Corrosion* 48 (1992): p. 882-890.
16. F. Cao, Z. Shi, G.L. Song, M. Liu, M.S. Dargusch, A. Atrens, *Corros. Sci.* 96 (2015): p. 121-132.
17. Z. Shi, J. Hofstetter, F. Cao, P.J. Uggowitzer, M. Dargusch, A. Atrens, *Corros. Sci.* 93 (2015): p. 330-335.
18. V. Raja, B.S. Padekar, *Corros. Sci.* 75 (2013): p. 176-183.
19. F.Y. Cao, Z.M. Shi, G.L. Song, M. Liu, M.S. Dargusch, A. Atrens, *Corros. Sci.* 96 (2015): p. 121-132.
20. S.P. Knight, K. Pohl, N.J.H. Holroyd, N. Birbilis, P.A. Rometsch, B.C. Muddle, R. Goswami, S.P. Lynch, *Corros. Sci.* 98 (2015): p. 50-62.
21. B.W. Pan, J.X. Li, Y.J. Su, W.Y. Chu, L.J. Qiao, *Corrosion* 68, 11 (2012): p. 1029-1036.
22. D. Tromans, R.S. Pathania, *Metall. Trans. A* 12, 4 (1981): p. 607-612.
23. G.M. Scamans, R. Alani, P.R. Swann, *Metall. Mater. Trans. A* 16 (1976): p. 443-452.
24. Q.N. Song, Y.G. Zheng, S.L. Jiang, D.R. Ni, Z.Y. Ma, *Corrosion* 69, 11 (2013): p. 1111-1121.
25. D.A. Hardwick, A.W. Thompson, I.M. Bernstein, *Metall. Trans. A* 14 (1983): p. 2517-2526.
26. D.A. Hardwick, A.W. Thompson, I.M. Bernstein, *Corros. Sci.* 28 (1988): p. 1127-1137.
27. L. Zhang, M. Du, Y. Li, *Corrosion* 68, 8 (2012): p. 713-719.
28. J.R. Scully, G.A. Young, S.W. Smith, *Mater. Sci. Forum* 331-337 (2000): p. 1583-1599.
29. X.M. Wang, X.Y. Liao, C.P. Ma, S.F. Zhang, Y. Liu, H. Chen, *Int. J. Mod. Phys. B* 29 (2015): p. 1540025.
30. G. Gou, M. Zhang, H. Chen, J. Chen, P. Li, Y.P. Yang, *Mater. Des.* 85 (2015): p. 309-317.
31. G.Q. Gou, N. Huang, H. Chen, H.M. Liu, A.Q. Tian, Z.C. Guo, *J. Mech. Sci. Technol.* 26 (2012): p. 1471-1476.
32. J. Chao, C. Hui, W. Xiaomin, M. Jijun, L. Hengkui, *J. Southwest Jiaotong Univ.* 48 (2013): p. 500-504.
33. W. Xiaomin, M. Chuanping, G. Guoqing, L. Yan, C. Hui, L. Hengkui, *Corros. Protect.* 34 (2013): p. 258-261.
34. Z. Shufang, W. Xiaomin, C. Hui, L. Xiaoyao, *J. Mater. Eng.* 43 (2015): p. 105-112.
35. ISO 2107:2007, “Aluminum and Aluminum Alloys-Wrought Products-Temper Designations” (Geneva, Switzerland: International Organization for Standardization, 2007).
36. ISO 12135:2002, “Metallic Materials-Unified Method of Test for the Determination of Quasistatic Fracture Toughness” (Geneva, Switzerland: International Organization for Standardization, 2002).
37. L.K. Berg, J. Gjonnes, V. Hansen, X.Z. Li, M. Knutson-Wedel, G. Waterloo, D. Schryvers, L.R. Wallenberg, *Acta Mater.* 49 (2001): p. 3443-3451.
38. A.M. Korsunsky, X. Song, J. Belnoue, T. Jun, F. Hofmann, P.F.P. De Matos, D. Nowell, D. Dini, O. Aparicio-Blanco, M.J. Walsh, *Int. J. Fatigue* 31 (2009): p. 1771-1779.
39. ISO 7539-6:2003, “Corrosion of Metals and Alloys-Stress Corrosion Testing - Part 6: Preparation and Use of Pre-Cracked Specimens for Tests Under Constant Load or Constant Displacement” (Geneva, Switzerland: International Organization for Standardization, 2003).

40. ISO 7539-8:2000, "Corrosion of Metals and Alloys-Stress Corrosion Testing - Part 8: Preparation and Use of Specimens to Evaluate Weldments" (Geneva, Switzerland: International Organization for Standardization, 2000).
41. M. Hauge, C. Thaulow, *Fatigue Fract. Eng. M* 16 (1993): p. 1187-1202.
42. ISO 7539-1:2012, "Corrosion of Metals and Alloys-Stress Corrosion Testing-Part 1: General Guidance on Testing Procedures" (Geneva, Switzerland: International Organization for Standardization).
43. Q.H. Li, *Materials Mechanics*, 6th ed. (Chengdu, China: Southwest Jiaotong University, 2006).
44. G. Weijie, "Research on Corrosion and Corrosion Fatigue Behavior of LC4 Aluminum Alloy" (Ph.D. diss., National University of Defense Technology, 2013), p. 44-48.
45. L. Anmin, W. Hui, G. Changqing, C. Ye, Y. Duo, *Mater. Rev.* 29 (2015): p. 84-88.
46. Q. Mingshan, J. Jinghua, S. Dan, Z. Lijuan, M. Aibin, *Corros. Protect.* 36 (2015) 677-683.
47. G. Gou, "Research on Corrosion Behavior and Residual Stress of A7N01 Welded Joints for High Speed Train" (Ph.D. diss., Southwest Jiatong University, 2013), p. 44-48.
48. W.Y. Chu, *Fracture and Fracture Under Environment*, 3rd ed. (Beijing, China: Science, 2000).